

OMAE2017-62244

INVESTIGATION OF SUSPENDED PARTICLES AROUND AN OBSTACLE IN VERTICAL PIPE FLOW – COMPARISON STUDY EXPERIMENTAL AND SIMULATION

Milad Khatibi
University of Stavanger (UiS)
Stavanger, Norway

Rune Wiggo Time
University of Stavanger (UiS)
Stavanger, Norway

Alexander Busch
Norwegian University of Science
and Technology (NTNU)
Trondheim, Norway

Stein Tore Johansen
SINTEF Material and Chemistry
, and Norwegian University of
Science and Technology (NTNU)
Trondheim, Norway

Dwayne Werner Martins
ENGIE E&P Norge
Stavanger, Norway

Md. Aminul Islam
Statoil ASA
Trondheim, Norway

Fionn Iversen
International Research Institute
of Stavanger (IRIS)
Bergen, Norway

ABSTRACT

Particle dynamics within Newtonian and viscoelastic shear thinning flows were investigated with a self-confined cloud of particles around an obstacle. Water and three aqueous Poly-Anionic Cellulose (PAC) solutions were test fluids. An experimental study of an upward vertical pipe was carried out using particle image velocimetry (PIV) techniques to measure the particle and liquid velocity profiles. The fluidized cloud height was measured for better assessing rheological and particle loading effects on particle interactions within liquid flows. It was observed that the dynamics of particles were closely associated with local shear rate, fluid rheology and particle loading. Additionally, it was noted that the slip velocity of particles was relative to the surrounding liquid and was high in regions with a high shear rate and depended significantly on the liquid rheological parameters. The experimental findings were compared against three-dimensional numerical CFD simulations. In the case of particle dynamics in the water sample, it was noted that the simulation results were comparable to the experimental observations. However, for PAC solutions, particles were completely flushed out from the computational domain. This was considered a consequence of inadequate drag and settling velocity formulation within the CFD model. These shortcomings of the drag model were rendered, as Newtonian drag laws were applied to a non-Newtonian fluid, and only used

background shear rates of the fluid flow field in estimating the local viscosity experienced by these particles.

Keywords: cloud of particles, vertical pipe/annulus, particle and liquid interaction, secondary flow, suspended particles, obstacle

INTRODUCTION

Understanding the physics behind turbulent particle-liquid flows is important for particle transportation within process systems involving particles and in particular, hole cleaning during hydrocarbon well drilling. The cuttings transport phenomenon in a vertical section is yet to be thoroughly investigated. In the larger hole vertical sections due to low fluid velocity, cuttings tend to stagnate. However, in practice it is seen that when the particle concentration increases, the interaction between particles also increases and as a result the effective shear rate increases and the apparent viscosity decreases. It is important to monitor the apparent fluid viscosity, as when the apparent viscosity increases the cuttings slip velocity decreases [1, 2]. The apparent viscosity in drilling muds affects the mud's cuttings carrying ability and the bottom hole hydrostatic pressure which impacts the pump pressure. Based on field observations in vertical sections, fluid flow is typically laminar above the bottom

hole assembly (BHA). As a result the slip velocity increases gradually as a wall or cuttings bed is approached. The particle interactions in vertical sections and its impact on slip velocity needs further comprehension in both Newtonian and, in particular, non-Newtonian fluids.

The primary function of mud additives to drilling fluids is as weight material. They provide density stabilization of the wellbore and hinder influx of fluids and gas, which could cause kick situations. Keeping these particles suspended in the fluids is also critical to avoid problems such as stuck downhole equipment, poor cementing of casings, lost circulation and avoid formation damage [3]. When drilling a well, weight materials such as barite, cuttings fines, and debris may settle in the drilling mud. As these particles are typically heavier than the liquid component, they tend to stagnate at various rates depending on their morphology and interaction with other particles. To keep these particles in suspension it is essential that the mud flow generates necessary frictional drag to prevent sagging. The slip velocity can be reduced by modifying the mud properties. Important is increasing the ratio yield point/plastic viscosity, and reducing the fluid behavior index thereby flattening the velocity profile. This flattened profile is good for hole-cleaning.

This study focuses on the dynamics of suspended particles flowing around an obstacle in a vertical upward flow. The obstacle was intended to mimic a BHA. This experimental setup has been considered a prototype for the impact of changing geometries along a vertical well. The advantage of the setup is to allow dynamical studies of a nearly stationary self-confined cloud of particles above an obstacle. The aim is to analyze characteristics of turbulence, physics, and models, by suspended particles in both Newtonian and non-Newtonian turbulent flows. The setup allows long time observation of the liquid-particle system under relatively constant flowing conditions. Also, this enables both overall and very detailed flow parameters to be determined and readily compared e.g. with CFD simulations.

The experimental findings were cross-examined against CFD simulations in order to examine key differences between experimental and computational results. Numerical CFD simulations were performed using Fluent R17.2. To study solid particles, the effects of drag, lift, virtual mass, turbulent dispersion and turbulent interaction were considered. Turbulent flow was modeled using the $k - \omega$ turbulence model on liquid and particle phases. In case of the PAC solutions, the fluid was considered in the simulation as purely viscous and modeled with Power-Law and Cross constitutive equations.

For the experiments, mono-sized particles were fed at a constant rate into the system. PIV technique was used to measure both particle and liquid velocities. Particle dynamics in both Newtonian (water) and three non-Newtonian poly-anionic cellulose (PAC) solutions were analyzed at room temperature (21°C) and atmospheric pressure (1.01 bar). As in vertical wells, hole cleaning is a question of pumping fluid fast enough to counteract the vertical slip of cuttings, thereby avoiding the cuttings concentration to increase. In the case of water, the flow was fully turbulent. As for non-Newtonian fluids, a laminar flow

rate was used, however high shear rate around the obstacle create turbulent like eddies.

State of art for modeling

During drilling, the cuttings carved out by the drill bit have to be transported and separated at the surface from the drilling fluid. The cuttings should be readily transported to the surface with minimum solids accumulation, as significant amounts of solids accumulation will affect both frictional pressure in the drilling fluid as well as increasing the possibility for stuck pipe. In order to predict the behavior of cuttings in drilling fluid, several physical phenomena must be accounted for.

In order to transport particles in vertical sections, drilling fluids with shear thinning behavior are used. A first challenge is to understand the rheology, which in the oil industry is usually fitted to the Herschel-Bulkley fluid model (Yield Power Law) these days [4, 5]. However, drilling fluids modeling practices used in field applications may differ from this simplified description in many ways, and may additionally show transient behavior, either due to thixotropy or viscoelasticity or both. The particles carried by the fluid will be subject to various hydrodynamic forces such as drag, lift, virtual mass, and lubrication. These are generally not well understood and hence we have studied [6-8] the effects of drag force. Particle dispersion is mainly a result of turbulence as well as inter-particle collisions. It is assumed that particle-particle interactions may be accounted for by generic granular theory models [9], but where the modeling of lubrication effects, impacting the collision cross sections, and hydrodynamic forces should be improved. The granular descriptions of particulate flows can also be extended to handle internal friction in compacted particle beds [9].

In laminar flows, granular dispersion is the main dispersive force. When flows become unstable, turbulent dispersion plays an integral role. When the flow becomes unstable turbulent dispersion will play a major role. In order to successfully simulate cuttings transport, a model must be capable of handling the turbulence in the bulk flow, as well as handling the turbulence in the boundary layer [10]. Furthermore, it was challenging to model the transition from laminar to turbulent flows [11], which is typically a complex phenomenon even for much simpler Newtonian flows. This demonstrates a clear need for generic wall functions [12] for turbulent non-Newtonian flows, however for simpler rheology models with zero yield stress (e.g. the Power Law model) standard wall scaling seems to be applicable [13].

EXPERIMENTAL FACILITY

Setup

Upward vertical pipe flow experiments were conducted at the multiphase-flow laboratory at the University of Stavanger, UiS. Figure 1 shows a sketch of the experimental setup. The (observation) test section has an inner diameter of 0.08 m and a length of 0.1 m with possible extension to 2.5 m. With a suitable

setting of liquid flowrate, the small spherical particles can be kept in the test section, and will form a self-organized cloud in the wake above a central cylindrical obstacle (item 2). The circular pipe (item 1) and the cylindrical obstacle are made of transparent plastic and acrylic, respectively. This allows for clear optical observation of suspended particles.

The liquid was pumped via the inlet by a small centrifugal pump (item 6) and the volumetric flow rate was measured by an electromagnetic flow meter (item 7). The liquid flow rate was logged using LabView program (National Instruments, NI-DAQ version 14.0). At the inlet, a flow straightener (item 4) was used to converge the flow into an approximately uniform velocity profile. The obstacle was held in the center of the pipe by using three sets of very strong magnet pairs. Three magnets were fixed into the obstacle, while the remaining three were outside the pipe wall, thus holding the obstacle in a stable position. The outlet of the vertical pipe was connected to a liquid tank (item 5) at atmospheric pressure.

Particle image velocity (PIV) technique was used to measure the fluid velocity and the particle velocity profiles. This technique was described in details in a previous study [14]. Two different optical arrangements were installed: (1) a SpeedCam MiniVis e2 camera (2500 *fps* in full resolution 512 × 512) equipped with a 532 *nm* green laser (Photon DPGL-2200). The laser plane was illuminated vertically through the center of the test section. Polyamide seeding particles (PSP-50 from DANTEC DYNAMICS) with a mean diameter of 50 μm was added to the liquids as tracer particles for measuring the field velocity profile. (2) A Basler A800-510um color camera (500 *fps* in full resolution 800 × 600) using a strong uniform white light LED panel giving background illumination of the test section. The spherical particles were tracked as they were moving upward along the plane jet, falling down at the center of the test section and sliding to the wall on the obstacle. The particles were relatively larger (1.2 *mm*) than tracer particles and having higher density (2500 kg/m^3) than the experimental fluids.

Fluids and Particles

Experiments were performed for water and aqueous solutions of Poly-Anionic Cellulose with concentrations of 1, 2, and also 3 *g/l*. Preparation of PAC solutions and rheology measurements were described in previous studies [14, 15]. Liquid samples were taken during each experiment for the rheology tests. Figure 2 represents the dynamic viscosity (μ) of the PAC solutions versus the shear rate ($\dot{\gamma}$). Power-law (PL) and Cross (Ca) models (Eq. (1) and Eq. (2)) were used for curve fitting of the rheology data.

$$\mu = \kappa \dot{\gamma}^{n-1} \quad (1)$$

$$\mu = \frac{\mu_0 - \mu_\infty}{1 + (c\dot{\gamma})^m} + \mu_\infty \quad (2)$$

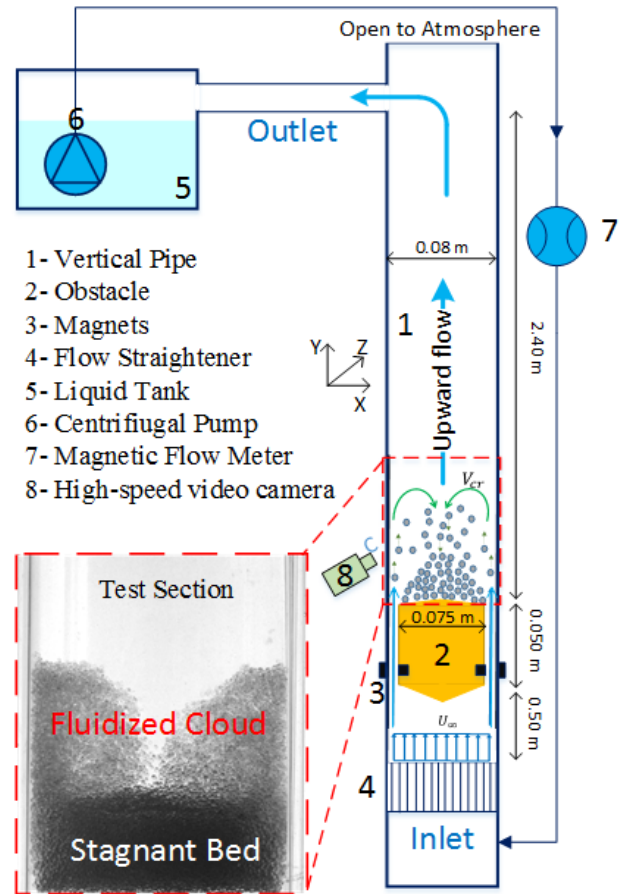


Figure 1. Schematic representation of experimental setup.

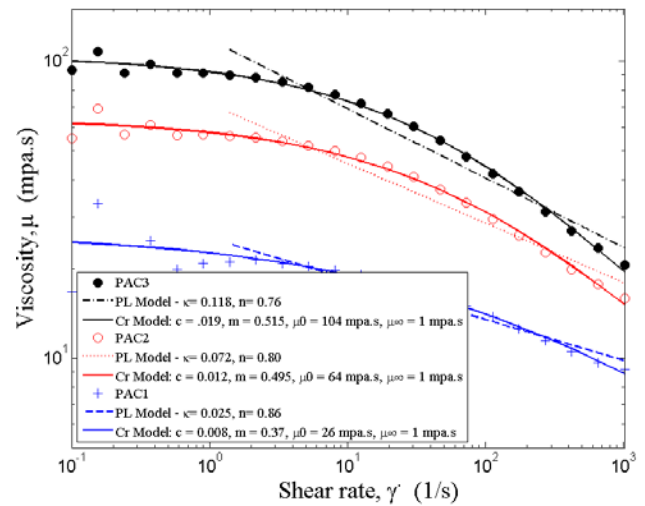


Figure 2. Rheology of PAC1, PAC2 and PAC3.

In addition to shear thinning behavior, PAC solutions may feature also viscoelastic properties. However, these effects have not been taken into account for the modeling part of this study.

Experiments with mono-sized particles, but different particle mass loadings (shown in Table. 1.) were carried out to investigate the impact of particle dynamics on turbulence characteristics. The density of the particles was 2500 kg/m^3 . The density and dynamic viscosity of the water were 998 kg/m^3 and $1 \text{ mPa} \cdot \text{s}$, respectively. All liquids were measured at room temperature (21°C) and atmospheric pressure (1.01 bar).

Test Procedure

Several tests were conducted at different fluid velocities with different particle loading for water and PAC solutions. The test matrix is represented in Table. 1. At the beginning of each test, the flow was allowed to stabilize for an hour in order to make sure that all bubbles had disappeared from the test section. Then the flow rate was recorded at a sampling frequency of 500 Hz over a period of 5 mins. The pipe Reynolds number was between 2.8×10^3 and 1.3×10^4 for water and between 9.3×10^0 and 2.1×10^2 for PAC solutions. The images of both single-phase (liquid only) and “two-phase” (liquid with particles) experiments were recorded by the camera system for further analysis.

To add the spherical particles in the test section, the particles were injected from the top opening of the experimental setup by a help of funnel and flexible pipe. The liquid flow rate was kept sufficiently low that the particle would fall down to the test section, but high enough to avoid falling through the annulus. Then the flow rate was increased to a certain rate as shown in the test matrix (Table. 1). The tests with PAC solutions were started at the highest polymer concentration with PAC3 and then diluted to PAC2 and subsequently to PAC1.

Table 1. Test matrix

Fluids	$d_p \text{ (mm)}$	$M_p \text{ (Kg)}$	$U_{sl-pipe} \text{ (m/s)}$
Water	1.2	0.05, 0.1, 0.2	0.035 - 0.169
PAC1	1.2	0.1, 0.2	0.014 - 0.101
PAC2	1.2	0.1, 0.2	0.014 - 0.101
PAC3	1.2	0.2	0.014 - 0.101

CFD simulation

CFD simulations were conducted in 3D on an 89882 cell hexahedral-polyhedral mesh using Ansys-Fluent R17.2. The entrance of the annular space was defined as velocity inlet and a cross-section at 0.3 m downstream of the obstacle was defined as pressure outlet. An Eulerian-Eulerian 2-fluid model combined with the kinetic theory of granular flow (KTGF) was used as a multiphase model. Drag, lift, virtual mass, turbulent dispersion and turbulent interaction were considered for the solid phase. Turbulence was modeled using the SST $k - \omega$ turbulence model for both the liquid and particle phase. In the case of the PAC solutions, the fluid was considered in the simulation as purely viscous and modeled with Power-Law and Cross constitutive equations. For the numerical solution of the model equations, pressure-velocity coupling was based on the Phase Coupled Simple algorithm, and 2nd order spatial and time discretization were utilized.

RESULT AND DISCUSSION

Fluid dynamics of water and polymer

Results from the experiments and CFD simulations without having particles are discussed in this section in order to identify the fluid dynamics behavior in the absence of particles. Figure 3 shows the time-averaged liquid velocity profiles based on experiments for water, PAC1, PAC2 and PAC3 at $U_{sl-pipe} = 0.045 \text{ m/s}$. At this velocity, the flow of water in the pipe was turbulent at $Re_{pipe} = 3.6 \times 10^3$. The flow of PAC solutions, even in laminar condition ($Re_{pipe} < 3.6 \times 10^2$), featured large eddies and local instabilities due to the wake from the annular flow “jet” around the obstacle.

The green laser was illuminated from the left side of the images. Due to the conic shape of the obstacle at the top, there was a shadow on the right side of the images as shown in Fig. 3. Also, the light was attenuated and more spread in the regions close to

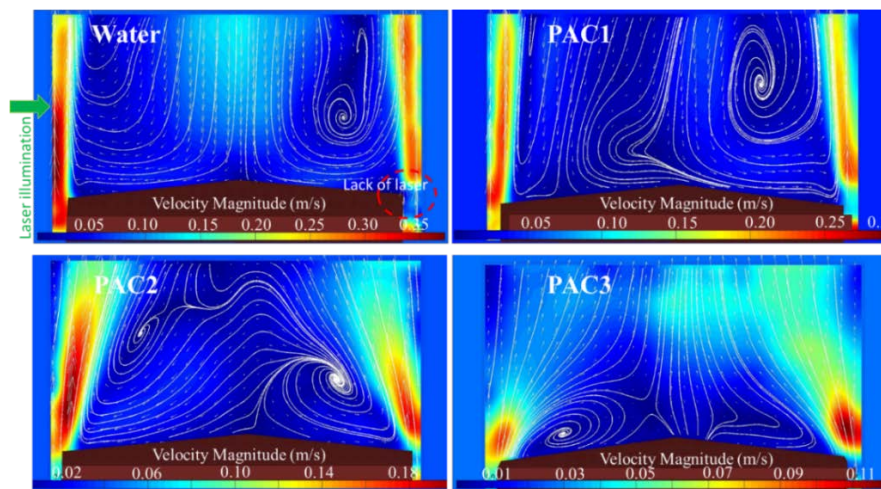


Figure 3. Single phase flow (water, PAC1, PAC2, PAC3) at $U_{sl-pipe} = 0.045 \text{ m/s}$, $U_{sl-annulus} = 0.37 \text{ m/s}$, Exp.

the right wall. In order to avoid too much weakening of the laser light, in some cases, the laser sheet was collimated into a parallel (non-diverging) sheet. In other cases, the laser sheet was uncollimated in order to cover a wider vertical section.

Figure 4 shows CFD prediction for the liquid velocity profiles for water, PAC1, PAC2, PAC3 at $U_{st-pipe} = 0.045 \text{ m/s}$. Qualitatively, the flow field is reproduced fairly well. However, due to the turbulence modelling, transient eddies are not resolved.

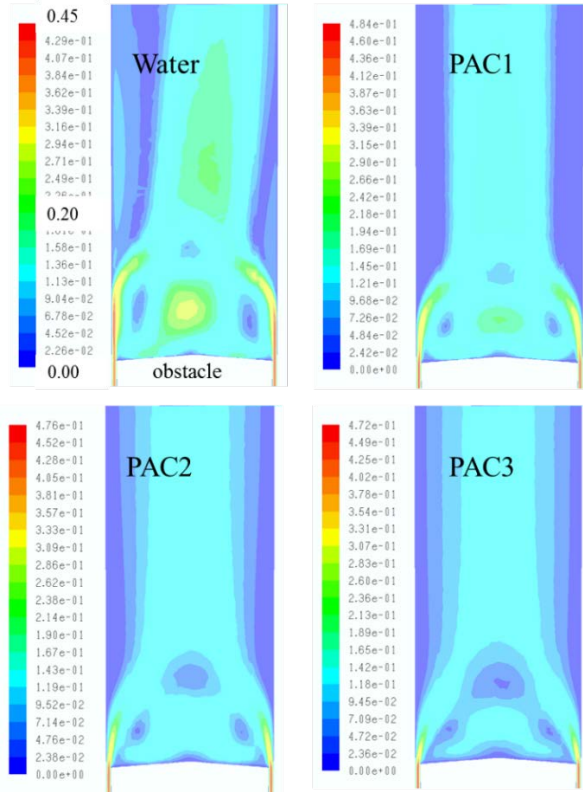


Figure 4. Single phase flow (Water, PAC1, PAC2, PAC3) at $U_{st-pipe} = 0.045 \text{ m/s}$, $U_{st-annulus} = 0.37 \text{ m/s}$, CFD (Ansys-Fluent 17.2, 3D, DP, pbns, Eulerian, SST $k - \omega$, steady state).



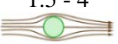

Suspended particles

The analysis of particle-liquid interaction in both Newtonian and viscoelastic shear thinning flows was concerned with the self-confined cloud of particles above the obstacle. The results indicate that the dynamics of particles are closely coupled with the local shear rate, the fluid rheology, and the particle loading. The pictures recorded using the white backlight LED panel, were used in this section. Figure 5 shows the spatial averaged (xy -plane cross section) volume fraction of suspended particles in different fluids flow and also the particle velocity profiles at $U_{st-pipe} = 0.045 \text{ m/s}$. The flow carrying the suspended

particles is turbulent. This is due to the shear rates in the overall fluid flow, but also local agitation caused by particle slip (interaction with the fluid), as well as particle-particle collisions. The pipe and obstacle geometry create a flow field with high velocity gradients and shear. As a consequence, the slip velocity of the quasi-stationary particles at the outer bed area relative to the surrounding liquid was high, while also the liquid itself undergoes considerable variation in shear rate. This resulted in a strong dependence on liquid rheological parameters. The particle Reynolds number in the test section where liquid was intensely shearing the particles was calculated by Eq. (3). The highest particle velocity indicated in Fig. 5 was used together with $U_{st-pipe}$ and $U_{st-annulus}$ in this calculation and the results are shown in Table. 2 and 3, respectively. Ideally, the particle Reynolds number should be calculated based on local velocities around the particle, but in order to get at least an estimate of the relative velocities, the superficial liquid velocities were used. In Table 2, the $Re_p = 366$ for water was indicating that the flow around the particles is expected to give cyclic shedding of ring vortices. The rings typically broke away, and drifted downstream in the wake flow, while again new rings were formed behind the particles. On the other hand, for $Re_p = 11$ for PAC1 in Table 2 and the $Re_p = 5, 8, 28$ in Table 3 for PAC1, PAC2, PAC3, we expected to have separation behind the particles but no shedding of vortices [16].

$$Re_p = \frac{\rho \times |U_p - U_l| \times d_p}{\mu \text{ (calculated from eq. 2.)}} \quad (3)$$

Table 2. Particle Reynolds number for the results in Fig. 5, using $U_{st-pipe}$ [16].

Fluid	$U_{st-pipe}$ (m/s)	U_p – highest velocity of particle from PIV images	Re_{l-pipe}	Re_p
Water	0.045	0.35	3.6×10^3	366 - 474 
PAC1	0.045	0.18	1.7×10^2	11 - 18 
PAC2	0.045	0.09	6.5×10^1	1.5 - 4 
PAC3	0.045	0.07	4.2×10^1	0.5 - 2 

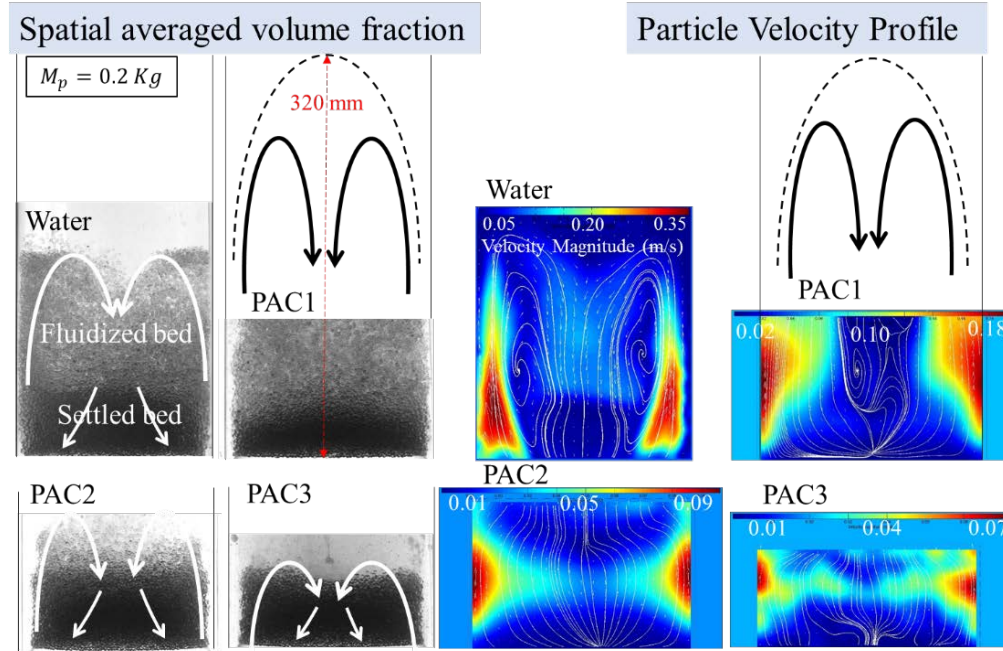


Figure 5. Suspended particles in water, PAC1, PAC2, PAC3 with $M_p = 0.2 \text{ Kg}$ at $U_{sl-pipe} = 0.045 \text{ m/s}$, $U_{sl-annulus} = 0.37 \text{ m/s}$, Exp.

Table 3. Particle Reynolds number for the results in Fig. 5, USING $U_{sl-annulus}$ [16].

Fluid	$U_{sl-annulus}$ (m/s)	U_p – highest velocity of particle from PIV images	Re_{l-pipe}	Re_p
Water	0.373	0.35	3.0×10^4	28 - 54
PAC1	0.375	0.18	1.9×10^3	16 - 45
PAC2	0.375	0.09	8.2×10^2	8 - 13
PAC3	0.370	0.07	5.7×10^2	5 - 7

CFD versus Experimental results

Figure 6 shows the CFD predictions for the particle volume fraction and particle velocity profiles for water, PAC1, PAC2, PAC3 at $U_{sl-pipe} = 0.045 \text{ m/s}$. In some cases, solid velocity was predicted in areas of zero volume fraction; however, this was a consequence of a plotting threshold of Fluent. Direct comparison of CFD and experimental results were not straightforward due to the following reasons.

- CFD results are depicted as xy -plane cross-sections, whereas experimental results show the frontal picture,

which may be considered as a spatial average of all possible xy -plane cross-sections of the test section.

- CFD results show the transient solution at $t = 10 \text{ s}$, for the water case and $t = 40 \text{ s}$ for the PAC cases, whereas experimental results represented the dynamic equilibrium observed at $t = 1 \text{ h}$.
- The rheology of the PAC fluids, or more precisely the Power-Law and Cross model coefficients (according to Eq. (1) and Eq. (2)), are based on rheometer measurements of flow curves, which may not represent the true/in situ fluid rheology in the experiment.
- The entrance length of the annular region is (0.05 m) is too short to obtain a developed velocity profile. Thus, velocity profiles of CFD and experiments at the end of the annular region are not fully consistent.
- The magnets keeping the obstacle in place have not been considered in the CFD model. However, they do have an effect on the shape of the fluid jet entering the test section.

In the water case, the simulation results indicated a maximum “bed height” equivalent to the experimental observations, seen from the images. For the PAC cases, no match was achieved. In the case of PAC2 and PAC3, the solids were flushed out of the computational domain during the time interval between $t = 40$ to 70 s . The solid velocity plots for $t = 40 \text{ s}$ indicated a particle transport along the annular fluid jet towards the exit of the domain. In the case of PAC1, it was expected that this might also happen at a later point in time due to the smaller apparent viscosity and thus higher settling velocity of the particle in the carrier fluid. A major flaw of the CFD model was the drag law, which, firstly, was not specifically tailored to shear-thinning

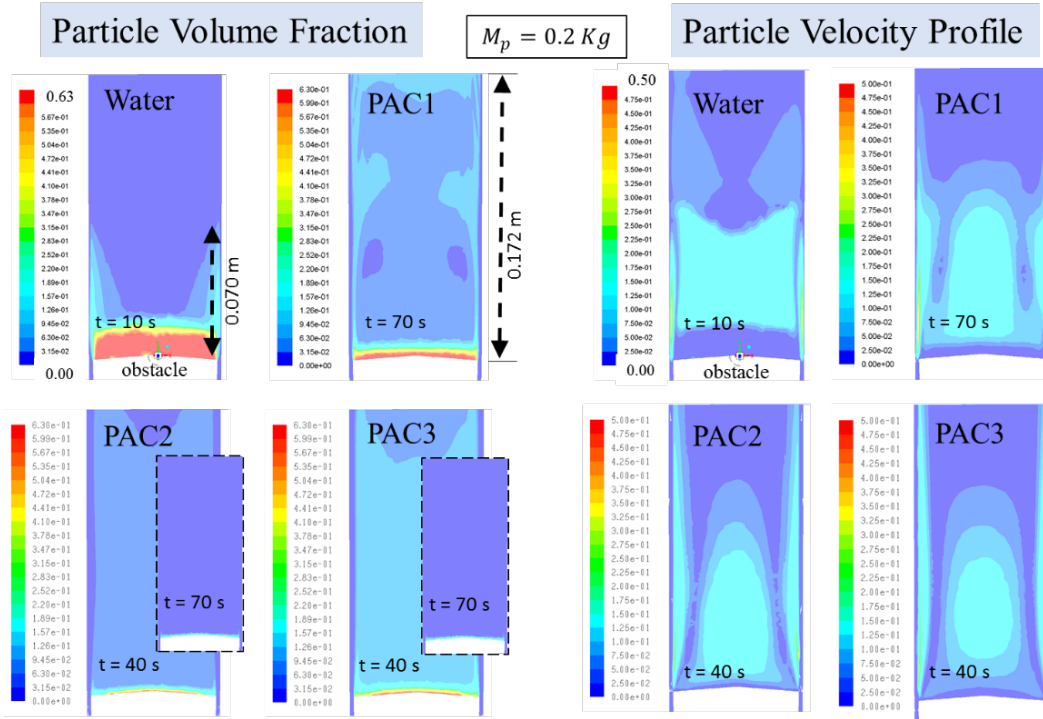


Figure 6. Suspended particles in water, PAC1, PAC2, PAC3 with $M_p = 0.2 \text{ Kg}$ at $U_{sl-pipe} = 0.045 \text{ m/s}$, $U_{sl-annulus} = 0.37 \text{ m/s}$, CFD (Ansys-Fluent 17.2, 3D, DP, pbns, Eulerian, SST $k - \omega$, transient).

rheology, and, secondly, only makes use of the global apparent viscosity based on the shear rate of the background fluid. Local, particle-induced shear rate and thus viscosity changes were not taken into account.

Another flaw of the CFD model was the assumption of non-existing interdependencies of non-Newtonian fluid rheology and turbulence. Non-Newtonian rheology was only taken into account via the molecular viscosity whereas the effect of turbulence is only taken into account by the corresponding models affecting the turbulent viscosity. This was due to the conventional but simplified RANS treatment where the viscosity is first considered constant and later made a variable by relating it to the shear rate as exemplarily shown in Eq. (1) and Eq. (2). Hence, terms representing the impact of fluctuations in strain rate on the “laminar” viscosity are ignored [17, 18].

Figure 7 shows the spatial averaged volume fraction of suspended particles in water, and the particle velocity profiles for different particle loadings at $U_{sl-pipe} = 0.045 \text{ m/s}$. The results indicated that the interaction between liquid and particles changed dramatically while changing particle loading. Apparently, and as known from theory, particles sometimes amplify turbulence while on other occasions cause weakening of turbulence. This also attributes to changes in the turbulent length scales, most importantly the eddy sizes. However, in these strongly inhomogeneous flows it affects the thickness of shear layers. Yet another factor here is the large variation of shear rate associated with impact of the non-Newtonian fluid behavior, see

Fig. 5. Figure 8 shows the CFD prediction for the particle volume fraction for water and the particle velocity profiles for different particle loadings at $U_{sl-pipe} = 0.045 \text{ m/s}$, and taken at time $t = 10 \text{ s}$ after initialization of the flow.

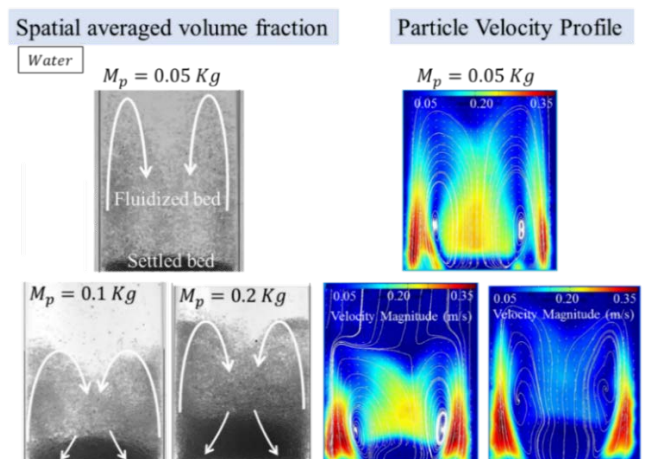


Figure 7. Suspended particles in water with $M_p = 0.05, 0.1, \text{ and } 0.2 \text{ Kg}$ at $U_{sl-pipe} = 0.045 \text{ m/s}$, $U_{sl-annulus} = 0.37 \text{ m/s}$, Exp.

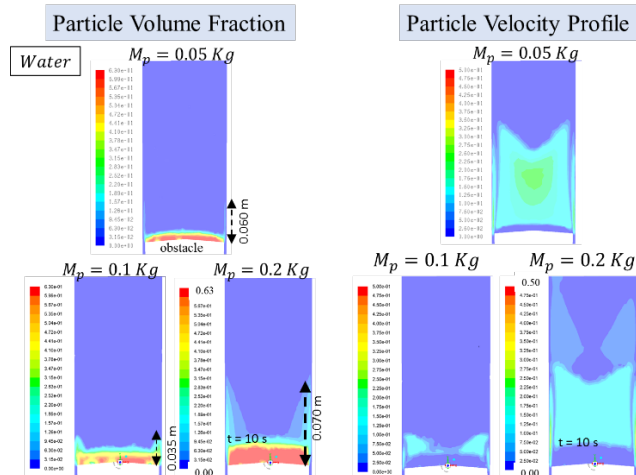


Figure 8. Suspended particles in water with $M_p = 0.05, 0.1$, and 0.2 Kg at $U_{sl\text{-}pipe} = 0.045 \text{ m/s}$, $U_{sl\text{-}annulus} = 0.37 \text{ m/s}$, CFD (Ansys-Fluent 17.2, 3D, DP, pbns, Eulerian, SST $k - \omega$, transient).

Figure 9 illustrates the fluidized “cloud height” versus superficial liquid velocities in the pipe for different fluids and different particle loadings. The height of fluidized cloud was measured using a ruler. The cloud height is a measure of the maximum vertical extent of the particle cloud and is significantly larger than the height of a stagnant bed. For the case of 0.2 kg particles the stagnant bed would have an average height of less than 27 mm , while the measured cloud height is as large as 300 mm . Still the observed cloud height give very valuable information of the vertical particle transport. From Figure 9 it can be seen, with the increase of $U_{sl\text{-}pipe}$, that the cloud height is increasing sharply at some critical flow rate. This is very pronounced for the PAC solutions, where the critical velocity increased with higher PAC number and effective viscosity. The impact of the particle loading is not dramatic, and appears to be rather complex. The particles need higher superficial velocities to get transported high up in the column, which is consistent with the lower viscosity and higher sedimentation velocity in water.

It can be seen, with the increase of $U_{sl\text{-}pipe}$, that the cloud height increased dramatically for water, while there was a sharp increase in cloud height in the case of PAC solutions from a critical liquid velocity. Further increase of $U_{sl\text{-}pipe}$, the particles suspended in liquid phase and flushed out from the test section.

We saw that the cloud height was relatively unchanged before reaching to this critical velocity (for PAC2 and PAC3 $U_{cr} \approx 0.06 \text{ m/s}$). PAC solutions exhibited higher apparent viscosity than water, causing the cloud height to be higher in PAC solutions than in water.

By comparing PAC1 with PAC2 and PAC3, one could consider the effect of viscoelasticity for PAC solutions, mostly for higher polymer concentrations (PAC2 and PAC3). As polymers are generally viscoelastic, elastic effects may “protect” the stagnant bed from the shearing annulus jet at low flow rates.

In addition, in the interstitial space between the particle, the local shear is low, resulting in very high local viscosity. This phenomenon will act to rigidify the stagnant bed and make entrainment difficult. With further increase of flow rate, the particles were sheared more and more by the annular jet flow, and the increased local turbulence caused the particles to become increasingly entrained into the jet. The particles stayed more in cloud suspension downstream the obstacle in PAC2 and PAC3 due to the combined effect of the higher viscosity and the viscoelasticity in polymer solutions. And for the same reasons, due to more annulus jet lift effect, the particle cloud rises higher in PAC1 than with PAC2 and PAC3. The critical liquid velocity was less and the cloud height was higher for PAC1 than PAC2 and PAC3.

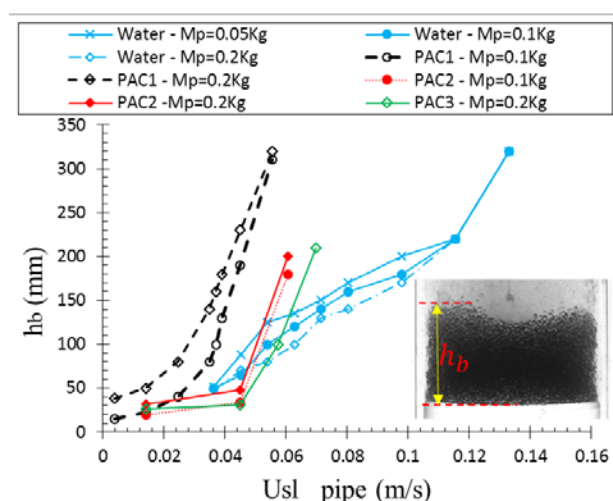


Figure 9. Fluidized cloud height, Exp.

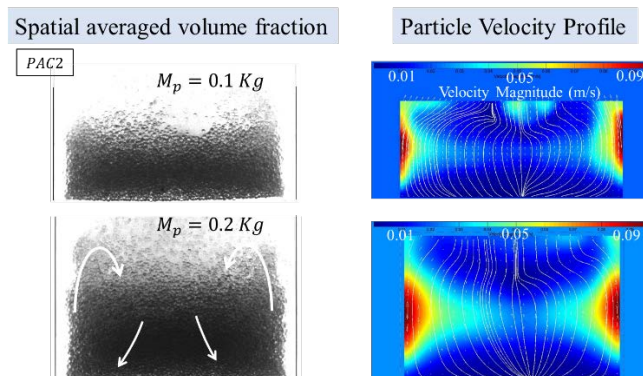


Figure 10. Suspended particles in PAC2 with $M_p = 0.1$ and 0.2 Kg at $U_{sl\text{-}pipe} = 0.045 \text{ m/s}$, $U_{sl\text{-}annulus} = 0.37 \text{ m/s}$, Exp.

For the PAC solutions, the observed cloud height seems to increase with increased particle loading. This is generally expected as we have more particles in the system. This is more clearly shown in Fig. 10 for particle loadings $M_p = 0.1$ and 0.2 Kg in PAC2 flow. We see from the figure that the compacted bed thickness may have been doubled in height while the measured cloud height had relative partial increments. For the lowest flow rate the cloud heights for PAC1 and PAC2 were very close to the theoretical bed thickness. In the water flow case, however, the loading effects seemed on the contrary. In the water case, both turbulence modulation effects and particle-fluid coupling may have impacted the flow behavior. Phenomena like particle clustering are very important in fast gas-fluidized bed systems, but was not observed here.

CONCLUSIONS

In this work, suspended particles for the Newtonian and non-Newtonian liquid flows were experimentally studied and analyzed by flow computations. Particle concentration profiles and liquid velocity profiles as well as the height of fluidized cloud were investigated and evaluated by means of numerical simulations. Based on combined experiments and simulations, the following conclusions are made.

- The dynamics of particles flowing in non-Newtonian fluids is closely coupled with the local shear rate, fluid rheology (e.g. local viscosity), vertical geometry, and the particle loading.
- The slip velocity of the particles, sheared by annulus jet, relative to the surrounding liquid was high. The liquid flow itself was rather unstable in regions with high strain shear rates, resulting in strong variations in local effective viscosities, dictated by the liquid rheological parameters.
- At low flow rates ($U_{sl-pipe} < 0.05 \text{ m/s}$), the stagnant bed in PAC2 and PAC3 solutions was “protected” from the shearing flow caused by annular jet by combined high interstitial viscosity in the particle bed and viscoelastic effects. At the higher flow rates the particles were entrained and dispersed by turbulence into the fluid volume downstream the obstacle. At higher particle loading, the fluidized cloud height for PAC solutions was higher than for the water.
- The CFD simulation demonstrated that particle transport in Newtonian flows may be fairly well predicted. However, particle transport in non-Newtonian flows requires additional modeling effort in order to describe e.g. interdependencies between rheology and turbulence or proper drag laws accounting for non-Newtonian rheology and the locally varying shear rate.

ACKNOWLEDGMENTS

The authors acknowledge the project [Advanced Wellbore Transport Modelling \(“AdWell”\)](#) for sponsoring this work. The AdWell project is funded by the Research Council of Norway and by the following industrial and university partners: Statoil ASA, ENGIE E&P Norge, IRIS, SINTEF, University of Stavanger (UiS) and NTNU. The authors thankfully acknowledge MSc students Kingsley U. Azuatalam and Sun Xianwei for providing valuable support during experiments.

NOMENCLATURE

BHA	bottom hole assembly
Ca	Cross model
CFD	computational fluid dynamics
Exp	experimental data
KTGF	kinetic theory of granular flow
PAC	Poly-Anionic Cellulose
PL	Power-Law model
SST	shear stress transport
c	Cross model parameter (-)
κ	consistency factor ($\text{mPa} \cdot \text{s}^n$)
m	Cross power index (-)
n	Power-Law index (-)
pbns	pressure based Navier-Stokes
d_p	median diameter of particles (m)
h_b	fluidized cloud height
M_p	particle mass load (Kg)
U_p	particle velocity (m/s)
$U_{sl-pipe}$	superficial liquid velocity in test section/pipe (m/s)
$U_{sl-Annulus}$	superficial liquid velocity in annulus (m/s)
PAC1, 2, 3	PAC 1 (g/l), PAC 2 (g/l), PAC 3 (g/l)
Re_{pipe}	liquid Reynolds number in test section (-)
μ	dynamic viscosity ($\text{mPa} \cdot \text{s}$)
μ_0	zero-shear viscosity ($\text{mPa} \cdot \text{s}$)
μ_∞	infinity shear viscosity ($\text{mPa} \cdot \text{s}$)

REFERENCES

- [1] Ranjbar, R., 2010, "Cuttings Transport in Inclined and Horizontal Wellbore," Master thesis, University of Stavanger, Norway.
- [2] Osei, H., 2009, "A Review of the Rheological Effects of Power Law Drilling Fluids on Cuttings Transportation in Non-Vertical Boreholes," PhD dissertation, African University of Science and Technology, Nigeria.
- [3] Omland, T. H., 2009, "Particle Settling in Non-Newtonian Drilling Fluids," PhD dissertation, University of Stavanger, Norway.

- [4] Institute, A. P., 2010, API Recommended Practice 13D – Rheology and Hydraulics of Oil-Well Drilling Fluids : 2010.
- [5] Busch, A., Islam, A., Martins, D., Iversen, F., Khatibi, M., Johansen, S., Time, R., and Meese, E., "Cuttings Transport Modeling-Part 1: Specification of Benchmark Parameters with a Norwegian Continental Shelf Perspective," Proc. SPE Bergen One Day Seminar, Society of Petroleum Engineers.
- [6] Jin, L., and Chenevert, M. E., 1994, "A Study of Particle Settling in Non-Newtonian Fluids—Part I: A New Method for the Study of Particle Settling in Drilling and Fracturing Fluids," *Journal of Energy Resources Technology*, 116(1), pp. 10-15.
- [7] Jin, L., and Chenevert, M. E., 1994, "A Study of Particle Settling in Non-Newtonian Fluids—Part II: Rheological Characterization of Polymer Solutions," *Journal of Energy Resources Technology*, 116(1), pp. 16-21.
- [8] Jin, L., and Penny, G. S., 1995, "Dimensionless Methods for the Study of Particle Settling in Non-Newtonian Fluids," *Journal of Petroleum Technology*, 47(03), pp. 223-228.
- [9] Laux, H., 1998, "Modeling of Dilute and Dense Dispersed Fluid-Particle Flow," PhD dissertation, Norwegian University of Science and Technology, Trondheim, Norway.
- [10] Trinh, K. T., 2009, "The Instantaneous Wall Viscosity in Pipe Flow of Power Law Fluids: Case Study for a Theory of Turbulence in Time-Independent Non-Newtonian Fluids," arXiv preprint Cornell University Library, <https://arxiv.org/ftp/arxiv/papers/0912/0912.5249.pdf>.
- [11] Trinh, K. T., 2010, "On the Critical Reynolds Number for Transition from Laminar to Turbulent Flow," arXiv preprint Cornell University Library, <https://arxiv.org/ftp/arxiv/papers/1007/1007.0810.pdf>.
- [12] Shih, T.-H., Povinelli, L. A., Liu, N.-S., Potapczuk, M. G., and Lumley, J., 1999, "A Generalized Wall Function," Technical Report, NASA Glenn Research Center, <https://ntrs.nasa.gov/archive/nasa/casi.ntrs.nasa.gov/19990081113.pdf>.
- [13] Trinh, K. T., 2010, "The Wall Shear Rate in Non-Newtonian Turbulent Pipe Flow," arXiv preprint Cornell University Library, <https://arxiv.org/ftp/arxiv/papers/1009/1009.3299.pdf>.
- [14] Khatibi, M., Time, R. W., and Rabenjafimanantsoa, H., 2016, "Particles Falling Through Viscoelastic Non-Newtonian Flows in a Horizontal Rectangular Channel Analyzed with PIV and PTV Techniques," *Journal of Non-Newtonian Fluid Mechanics*, 235, pp. 143-153.
- [15] Khatibi, M., Potokin, N., and Time, R. W., 2016, "Experimental Investigation of Effect of Salts on Rheological Properties of Non-Newtonian Fluids," Nordic Rheology Conference 2016, University of Helsinki, Finland.
- [16] Southard, J., 2006, "An Introduction to Fluid Motions, Sediment Transport, and Current-Generated Sedimentary Structures," Massachusetts Institute of Technology (MIT) OpenCourseWare, <http://ocw.mit.edu/courses/earth-atmospheric-and-planetary-sciences>.
- [17] Pinho, F., 2003, "A Model for the Effect of Turbulence on the Molecular Viscosity of Generalized Newtonian Fluids," 17th International Congress of Mechanical Engineering, Brazilian Society of Mechanical Sciences and Engineering (ABCM), Sao Paulo.
- [18] Gavrilov, A. A., and Rudyak, V. Y., 2016, "Reynolds-Averaged Modeling of Turbulent Flows of Power-Law Fluids," *Journal of Non-Newtonian Fluid Mechanics*, 227, pp. 45-55.